Improved critical temperature of superconducting plasma-enhanced atomic layer deposition of niobium nitride thin films by thermal annealing

Liang Tian, Ivane Bottala-Gambetta, Victor Marchetto, Manoël Jacquemin, Alexandre Crisci, Roman Reboud, Arnaud Mantoux, Frédéric J. Mercier, Gregory Berthomé, André Sulpice, et al.

Soumis dans Thin Solid Films, Elsevier, 2020

Improved critical temperature of superconducting plasma-enhanced atomic layer deposition of niobium nitride thin films by thermal annealing

Liang Tian[1], Ivane Bottala-Gambetta[1], Victor Marchetto[1], Manoël Jacquemin[1], Alexandre Crisci[1], Roman Reboud[1], Arnaud Mantoux[1], Gregory Berthome[1], Frédéric Mercier[1], André Sulpice[2], Laetitia Rapenne[3], François Weiss[3], Carmen Jimenez[3], Elisabeth Blanquet[1]

1. Univ. Grenoble Alpes, CNRS, Grenoble INP*, SIMaP, 38000 Grenoble, France.
2. Univ. Grenoble Alpes, CNRS, Institut Néel, 38000 Grenoble, France
3. Univ. Grenoble Alpes, CNRS, Grenoble INP*, LMGP, 38000 Grenoble, France

* Institute of Engineering Univ. Grenoble Alpes.

Keywords

Atomic layer deposition
Niobium nitride
Plasma
Thin film
Superconducting properties

Abstract

The efficiency of the superconducting radio frequency cavities composed of Nb required the deposition of thickness-controlled multilayer coatings of superconductor-insulator-superconductor (S-I-S) on the internal surfaces of the cavities. Herein, we report the plasma-enhanced atomic layer deposition of carbon-free NbN (50 µm thick), followed by a thermal treatment, to obtain the superconducting layer in the S-I-S structure. Using (tert-butylimido)-tris(diethylamino)-niobium as the niobium precursor and H_2 and NH_3 plasma as reactive gases, the deposition and annealing parameters were optimized by studying their effects on the film properties (crystallinity, density, and composition). We demonstrated that the superconducting critical temperature (Tc) can be improved after thermal annealing up to 13.8 K, a value compatible with the targeted application. In addition to the expected densified layers and increased grain size, we observed a partial transformation of the oxide present in the as-deposited layer into niobium oxynitride, which could indicate the origin of the improvement of the superconducting properties. With low carbon and oxygen impurity concentrations in the films, this study contributes to the understanding of the relationship between the structure, composition, and superconductivity in NbN.

1. Introduction

Niobium nitride (NbN) thin films exhibit excellent physical, chemical, and electrical properties that are adaptable to applications such as hard surface coatings [1–4] or superconducting radio frequency cavities. NbN thin films can be deposited by physical vapor deposition (PVD), chemical vapor deposition (CVD), and atomic layer deposition (ALD). ALD, which is based on a surface reaction leading to a self-limiting, layer-by-layer growth, is the most favorable method for growing conformal films on high-aspect-ratio structures at relatively low temperatures [5]. The importance of the ALD process for obtaining NbN film layers depends on the potential improvement of the efficiency of Nb-based superconducting radio frequency cavities by coating the internal surfaces with a multilayer coating of superconductor-insulator-

superconductor [6,7]. This application requires a controlled preparation of an atomically precise thickness of NbN on a complex surface.

The deposition of NbN by thermal ALD has been generally performed by alternatively pulsing $NbCl_5$ and NH_3 [8]. In some cases, an intermediate Zn pulse, which is used as an additional reducing agent to increase the Nb reduction from niobium(V) chloride ($NbCl_5$) to niobium(III) nitride (NbN), was also introduced between the $NbCl_5$ and NH_3 pulses. The resulting NbN films exhibited a resistivity reduction by a factor of 2 [9,10]. The intermediate Zn pulse improved the superconducting critical temperature (Tc) from 4 K to 7.5 K [11]. Nevertheless, the reducing power of the reactive gases like NH_3 used in thermal ALD is insufficient to obtain stoichiometric nitrides from a metal precursor [12]. Therefore, plasma-enhanced ALD (PEALD) is used to greatly improve the quality and the density of the films [13]. Furthermore, organometallic and coordination complex precursors are often preferred because halide precursors are susceptible to equipment corrosion and environmental issues.

A prospective molecular precursor for NbN deposition is (tert-butylimido)-tris (diethylamino)-niobium(V) (TBTDEN), which can be combined with H_2 plasma [14,15]. However, in this case, the nitrogen originates from the precursor and it is difficult to prevent carbon contamination in the films. In other cases, the TBTDEN is combined with N_2 [16] or H_2/N_2 [17] plasma as the reducing agent to form NbN. Efforts have been focused on the evolution of film properties with the process parameters (plasma duration, temperature) and film thickness. Extremely interesting results (Tc: ~14 K for the ~30 nm thick film) have been reported using TBTDEN/H_2 [15,18] or TBTDEN/H_2/N_2 [17,19]. Several authors [14,18] reported that the films may contain relatively high amounts of oxygen and carbon, up to 50 at%. However, high impurity levels make it difficult to make definite conclusions on the relationship between material properties and the superconductivity. Nitrogen atoms can be substituted by carbon to form a solid solution of NbCN in the full composition range. In this case, the structure remains cubic with an

improved Tc value for 15–40 at% C [20–22]. Nitrogen atoms can be also substituted by oxygen. The oxynitride NbON remained cubic and the Tc increased as the oxygen concentration approached 20 at% [23–25]. In this study, we used a non-conventional approach (termed supercycle), which consists of a pulse of TBTDEN, followed by a pulse of H_2 plasma. In addition, we added another pulse of NH_3. The objective of the supercycle was to break the TBTDEN ligands due to the H_2 plasma to facilitate the surface chemical reaction with NH_3 in order to limit the incorporation of carbon and oxygen in the film. This approach was already verified in the PEALD process of the AlN thin films [26]. After testing the superconducting properties of the as-deposited PEALD films, a post-deposition annealing in Ar was also performed to investigate its influence on the quality of the films and on the Tc. In this paper, the superconducting properties of the films were evaluated using the value of the Tc, with the objective of obtaining a Tc above 9 K, which is the Tc of the pure niobium.

2. Experimental

2.1 NbN films ALD growth

NbN thin films were grown on the (100) silicon substrates in a Picosun R-200 Advanced ALD system, which features thermal ALD and PEALD equipped with an inductively coupled remote plasma ~~(ICP)~~ source. TBTDEN (99.99%, STREM Chemicals) was used as the Nb precursor. The Nb precursor container was maintained at 90 °C and delivered to the system with a precursor Picohot™ boosting system. The boosting system used a Venturi effect generated in the precursor source by the carrier gas to increase or boost the amount of precursor injected into the ALD reactor, substantially improving the transfer of the low vapor pressure material from the cylinder to the substrate surface. Each of the substrates were previously cleaned in an ultrasonic bath in acetone and isopropanol for 15 min before the deposition.

We used N_2 (99.9999%, Air Liquide) as carrier gas to dilute the NH_3 (99.999%, Air Liquide). The NH_3 and N_2 flow rates were maintained at 100 and 120 mL/min, respectively. The pulse time of the niobium precursors was controlled between 0.5 and 4 s with the boosting function. The NbN growth was obtained by sequentially exposing the heated substrate to the precursor gases in the following order: TBTDEN, N_2 purge/4 s, remote H_2 plasma/variable time, N_2 purge/4 s, NH_3/5 s, and N_2 purge/4 s. This reacting gas steps plasma H_2/thermal NH_3 listed in Table 1 as process 1 enable the separation of the surface activation by H_2 from the reaction step with NH_3. The substrate temperature was varied between 200 and 400 °C to determine the ALD window. Herein, 2000 cycles were performed in all the experiments. In normal operation, the plasma is subjected to an inductive regime; however, a capacitive regime could appear when the injected gas flow is large. These capacitive discharges could damage our reactor; therefore, the gas flow rate was selected within the limit of our reactor [26].

The maximum gas flow rate in the induction mode is a function of the electrical power delivered by the generator. In this study, the plasma power was fixed at 2800 W, which allows a wide range of flow variation. The Ar flow (80 mL/min) was used as a carrier gas and the H_2 flow rate used to generate the reducing plasma was varied from 40 to 170 mL/min. In this setup, the plasma is functioned in an inductive regime [26].

NbN films were also grown by a simpler ALD cycle consisting of an NH_3 plasma (170 mL/min) and an Ar carrier gas (80 mL/min). This alternative ALD route constitutes process 2 in Table 1.

Table 1: Parameter values for ALD processes 1 and 2.

		ALD Steps						T (°C)
Process 1	ALD cycle	TBTDEN	Purge N_2	Plasma H_2 2800 W	Purge N_2	NH_3	Purge N_2	240–400
	Pulse duration (s)	0.5–4	4	12 or 24	4	5	4	
	Rate flow (mL/min)	Boosting function*	120	H_2: 40–170 Ar: 80	120	NH_3:100 N_2:120	120	
Process 2	ALD cycle	TBTDEN	Purge N_2	Plasma NH_3 2800 W	Purge N_2			240–400
	Pulse duration (s)	1	4	12 or 24	2			
	Rate flow (mL/min)	Boosting function*	120	100 for NH_3 80 for Ar	120			

* The boosting function is performed with two N_2 flow rates: half the pulse time at 80 mL/min then 600 mL/min

After the deposition, the films were annealed in a tubular furnace in a controlled Ar atmosphere (99.9999 %, Air Liquide) between 800 and 1200 °C inside an alumina tube with a heating rate of 20 °C/min. The annealing duration was varied between 10 and 60 min. The gas flow rate and base pressure during annealing were 200 mL/min and 800 Pa, respectively.

2.2 NbN films characterization

The composition of the NbN films was determined by an Electron Probe Micro-Analyzer (EPMA) using a Cameca SX50 controlled by an SAMx software. Niobium, nitrogen, carbon, and oxygen were analyzed at 3, 5, 7 and 10 kV acceleration voltage, respectively. The thickness and composition of the thin films were extracted from the measurements using the Stratagem software.

The XPS (X-ray Photoelectron Spectroscopy) analyses were conducted using a Thermo Scientific™ K-Alpha™ XPS spectrometer. The sample surfaces were irradiated with Al Kα

radiation at 15 kV for a current of 20 mA. To correct any charging effect, all the binding energies were calibrated to the C-C component of the C 1s core spectrum at 285.0 eV. Analyses were conducted at 90° angles between the sample surface and the analyzer, corresponding to an analyzing depth of 8–9 nm. An Ar ion gun (3 keV) was used to etch the surface for 5 min to remove the surface contamination and probe the in-depth composition of the NbN films. Peak deconvolutions were performed using Thermo Scientific Avantage software.

Field emission gun scanning electron microscopy (ZEISS Ultra-55) was used to characterize the surface morphology of the NbN layers. High-resolution transmission electron microscopy (HRTEM) was performed on samples with a JEOL 2010 microscope operating at 200 kV. The samples were prepared for TEM observation by the grating method. X-ray diffraction (XRD) patterns were collected with a Siemens (Bruker) D5000 diffractometer equipped with a Cu source (λ= 1.5406Å) according to the Bragg-Brentano configuration. The θ–2θ scans were performed between 20° and 75°. X-Ray Reflectivity (XRR) was performed with the same diffractometer operating in the reflectivity mode. Fitting with X-Pert Reflectivity software enables evaluation of the film thickness and density.

Magnetic measurements were performed in the field perpendicular to the largest plane of the sample using a commercial Metronique Ingenierie Superconducting Quantum Interference Device Device (SQUID) magnetometer with a sensitivity of of 10^{-10} A.m^2 at low field. After cooling the sample at zero field, the magnetization was first measured at 2 K by increasing the field to to 795.6 A/m. The sample was then cooled at constant field by increasing (Zero Field Cooled) and decreasing (Field Cooled) the temperature. The deviation of these curves with the normal state at high temperature was used to determine Tc.

3. Results and discussion

3.1 ALD window

To optimize the NbN growth process under the conditions described in process 1, two steps were conducted: 1) the TBTDEN pulse duration, and 2) the substrate temperature were varied. Only these two parameters were considered because they strongly depend on the precursor nature and chemistry. The other step durations (purge, H_2 plasma, and NH_3 step) were optimized in a previous study using the same reactor [26]. We varied the TBTDEN pulse duration between 0.5 and 4 s using the Picohot^{TM} boosting function. All other parameters were fixed at the values specified for process 1 in Table 1. The optimal pulse duration corresponds to the precursor volume required to react with the entire active surface, characterized by a growth per cycle (GPC) value independent of the pulse duration. The deposition temperature was fixed at 350 °C to optimize this parameter. We postulated that 1 s of the TBTDEN using the boost function is the minimum time required to obtain a reproducible and constant GPC of ~0.01 nm/cycle. As expected, a further increase in the TBTDEN pulse duration does not alter the GPC in a self-limited ALD process. Therefore, 1 s is sufficient for the reactions to occur in the ALD mode.

In the second step, the deposition temperature range was adjusted to maintain a constant GPC independent of the substrate temperature, also called the ALD window. We varied the substrate temperature between 240 and 400 °C kept all the other parameters for process 1 constant, as shown in Table 1. The GPC and film density as functions of the substrate temperature are shown in Fig. 1. As the substrate temperature increased, the GPC decreased initially, then stabilized to 0.015 nm/cycle between 350 and 380 °C. This GPC value could be defined as the ALD window in our process. A further increase in temperature leads to a decrease in the GPC. The GPC obtained by our process is lower than the value obtained by Ziegler et al. [15], i.e., a saturated GPC of 0.045 nm/cycle for films deposited at 350 °C, using TBTDEN/H_2 plasma. This difference in the GPC might be due to the different growth conditions (such as additional step of NH_3) and consequent different film compositions (low amount of C and/or O impurities). For instance, Sowa [17] demonstrated that using TBTDEN and plasma N_2/H_2, the ALD window was not

observed and an increase in GPC as a function of the substrate temperature was found. Hinz et al. [27] reported a slight increase in GPC from 0.065 to 0.072 nm/cycle between 200 and 350 °C when using another molecular precursor in the same family as the niobium precursor, i.e., (tert-butylimido)-tris (dimethylamino)-niobium Nb(N-t-Bu)$(NMeEt)_3$ (TBTMEN).

Importantly, the film density increased continuously as the substrate temperature increased to 350 °C (Fig. 1); further increase in the substrate temperature does not significantly alter the film density. This relationship with temperature may be associated with a low concentration of incorporated impurities like C and O above 350 °C. Another possible explanation is that an increase in the substrate temperature thermally accelerates the chemical reactions. Therefore, denser films are formed, leading to a decrease in GPC. The GPC and film density values in the ALD window for process 1 are 0.015 nm/cycle and 7 g/cm^3, respectively. For comparison, the bulk NbN density is 8.47 g/cm^3 [28].

The ALD growth using process 2 was performed at a deposition temperature of 350 °C to evaluate the effect of the ammonia plasma. The GPC and the NbN thin film density obtained in these conditions are 0.0245 nm/cycle and 7.2 g/cm^3, respectively. The PEALD deposition of NbN using an NH_3 plasma has a higher growth rate and a slightly higher density, which might be due to the higher reducing power of NH_3 as compared to that of the H_2 plasma.

The films deposited using process 1 (H_2 plasma/NH_3) and process 2 (NH_3 plasma) were characterized by XPS to assess the complete decomposition of the precursor. Fig. 2 shows the C 1s peak of the NbN samples deposited at 330 and 350 °C by process 1, and at 350° C by process 2. The peak located at ~282.8 eV was assigned to the presence of C-Nb bonds because only the metal-carbon bonds could be assigned to such a low binding energy [29]. Fig. 2 shows that the area of the carbon peak is most pronounced in the sample deposited at a lower temperature (330 °C) by process 1. The presence of the C-Nb bonds suggests an incomplete reaction between TBTDEN and H_2 plasma, NH_3 reactive. At 350 °C, the intensity of this peak decreases, whereas

no C-Nb bonds exist in the sample deposited by the NH_3 plasma (process 2) at the same temperature. Therefore, we fixed the substrate temperature at 350 °C for the remainder of the study to have carbon-free NbN samples.

Based on the literature, deposition was only obtained with plasma assistance. In thermal ALD, the NH_3 step itself is not sufficiently reducing to ensure deposition from TBTDEN, which has previously been reported by Ritala et al. as Nb chloride precursors [12].

After parameter optimization, to study the influence of the different plasmas on the superconducting properties of the NbN films, four samples were deposited for two plasma durations using processes 1 and 2 for 2000 ALD cycles. The measured thickness of all samples is between 30 and 50 nm.

- Samples S1 and S2 were deposited using process 1 with H_2 plasma pulse durations of 12 and 24 s, respectively, followed by an NH_3 step of 5 s.
- Samples S3 and S4 were deposited using process 2 with NH_3 plasma pulse durations of 12 s and 24 s, respectively.

We studied these four different experimental conditions and repeated each experiment five times. No differences were observed among the samples deposited under identical conditions. Henceforth, we used the same label for the same deposition conditions.

3.2 Crystallographic phase

θ–2θ scans were performed on samples S1 to S4 and results are shown in Fig. 3. The samples were tilted slightly with 2° to decrease the contribution of the Si substrates. The peak centered at 70° is due to Si substrates after tilting. Peaks were ascribed to the (111), (200), (220), and (222) diffraction planes of the δ-NbN cubic fcc structure (ICDD: 04-004-2895). This reported phase is associated with a chemical composition of $NbN_{0.98}$ with a lattice parameter of a = 0.439 m [30].

From the HRTEM images and selected area electron diffraction (SAED) of sample S2 shown in Fig. 4a and 4c, the films were not completely crystallized, whereas the NbN cubic phase with an Fm-3m structure was embedded in a matrix of the amorphous phase. The estimated mean size of the crystallites is 10 nm.

3.3 Critical temperature

The superconducting behavior was tested for all the samples and a superconducting transition at 3 K was only detected for sample S2. All other samples had a Tc below 2 K. To understand the origin of these low values of Tc and to increase the superconducting properties of the films, the thermal treatments in the Ar atmosphere were conducted at different temperatures ranging from 800–1200 °C for a duration between 10 and 60 min. The samples annealed in the Ar atmosphere at 1000 °C for 30 min exhibited the optimum Tc; Fig. 5 shows the measurements (SQUID method) for the same set of samples, which are renamed with an "A" to distinguish the as-deposited samples. The Tc of all the samples significantly improves and sample S2-A has the highest Tc (13.8 K), which is the same as the highest value reported in the literature for samples prepared by a thermal or a plasma-enhanced ALD process. This value was validated by R(T) measurements. S3-A reveals a Tc of 11.6 K, which is similar to that of S1-A (11.1 K). S4-A exhibits the lowest Tc value (10.1 K). The evolution of the Tc of all our samples with annealing differs from that of several previously published results, where it is shown that annealing lowers the Tc [19, 31]. Other publications show that annealing between 800 and 1000 ° C increases the Tc of the NbN samples [32–34].

To understand why Tc improved significantly after annealing and to establish the contribution of film crystallinity, density, or composition, we characterized the as-deposited and annealed samples by SEM, XRD, XPS, and EPMA.

3.4 Effect of annealing in argon

SEM was used to examine the surface morphology of the samples. No cracks were observed in any sample after thermal annealing. Fig. 6 shows the SEM images of sample S2 before and after annealing. Sample S2 consisted of small round grains and no difference in the surface morphology was observed before and after annealing. The same result was observed for all the samples. However, we noticed an increase in the nanocrystal size (lateral size) from 10 nm (Fig. 6a) before annealing to ~30 nm after annealing (Fig. 6b). This result was confirmed by HRTEM (Fig 4b). The crystallinity of the layer was increased (Fig 4d) and the mean size of the crystallites after annealing was 30 nm. This reduction in the grain boundary densities could contribute to improved superconducting properties after annealing.

Fig. 7 depicts the θ/2θ diffraction patterns of samples S1–S4 after annealing. Diffraction peaks could be attributed to the same δ-NbN cubic structure (ICDD: 04-004-2895 with a = 4.39 Å). However, the crystallinity of all the samples increased significantly, as indicated by the strong (111) peak compared to sample before annealing. This result is consistent with the increase in the signal intensity in SAED (Fig. 4d), as previously discussed. All the samples have a (111) preferred orientation. The lattice parameters of samples S1 to S4 before and after annealing were calculated and plotted in Fig. 8.

The lattice parameters are smaller than the theoretical ones (a = 4.39 Å), as recorded by selected ICDD 04-004-2895 crystallographic data. The lattice parameter of the as-grown samples is extremely small for S1, S2, and S3, and is similar to the theoretical value for S4. The peak shift observed in Fig. 3 was attributed to the composition difference rather than to the stress in the film. The lattice parameters of the annealed films exhibit similar values. From this perspective, no differences among the four samples could be established. Previous reports [18, 35–37] on NbN thin films obtained by PVD or ALD processes demonstrated that the superconducting properties of the NbN thin films are strongly dependent on its lattice parameter; moreover, a larger value leads to a higher Tc. The lattice parameter depends on the chemical composition and vacancies of

Nb or N, and the presence of O reduces the lattice parameter [31]. In our study, the four annealed samples exhibited extremely similar lattice parameters after annealing. Therefore, there is no correlation between Tc and the lattice parameter, which contradicts other reports. We can conclude that, apart from the lattice parameter, there are other more significant factors that influence the Tc of the films.

The film density was measured by XRR for samples S1–S4 before and after annealing. Fig. 9, shows that the density of the samples increased after annealing and S2 exhibited the highest density among all of the samples.

The stoichiometry and composition of the films were also directly associated with the superconducting properties of NbN. It is important to achieve an optimal Nb/N ratio for the highest Tc, and to understand the contribution of carbon and oxygen. The chemical compositions of the NbN samples before and after annealing were measured by the electron probe microanalyzer (EPMA). The atomic ratios of Nb/N and the at% O atomic concentrations are shown in Fig. 10a and b. Annealing in Ar improved the stoichiometry of the NbN, approaching values close to 1. Importantly, annealing did not increase the oxygen content in the films, which remained low (from 14 at% to 5 at%). From this composition analysis, the origin of the low Tc (< 3 K) before annealing could be correlated with the absence of carbon in our films. This correlates with the results obtained by Proslier et al. where the NbN films grown from $NbCl_5$ (i.e., carbon-free films) also exhibit a Tc value below 3 K [11]. The carbon enhanced the Tc and, based on existing information in previous studies on the ALD synthesis of NbN [14–19], the presence of carbon as an impurity in the classical ALD process could significantly impact the superconductivity. Therefore, the improvement of the Tc of our carbon-free samples after annealing is related to another parameter. Hence, XPS was performed on sample S2 before and after annealing, which demonstrated the optimum superconducting properties. The samples were first etched by argon ions for 5 min. The spectra were fitted by Gaussian-Lorentzian functions.

The fitting for the Nb 3d state took into account a spin orbital splitting of 2.72 eV of the 3/2 and 5/2 components with an area ratio of 2:3. The Nb 3d spectrum was fitted with the three chemical states of Nb according to a report by Halbritter et al. [38] and the values of the binding energies of Nb 3d5/2 are indicated in Fig. 11. These three components were assigned to Nb-N (204 eV), Nb-oxynitride (205.3 eV), and Nb-oxide (207.1 eV), which were also retrieved in N 1s and O 1s spectra. Similar results were observed by Ziegler for the optimized conditions and they fitted the Nb 3d spectra with four contributions; the additional one was attributed to Nb-carboxide, which was not observed in our case [15]. In the O 1s spectra, the contributions of niobium oxide and niobium oxynitride are observed. Notably, a third contribution (blue line in the XPS spectra) was not clearly identified. For this contribution, the signature of Nb-carbonitride might be considered in the O 1s spectra, but no carbon (C 1s) was observed.

It can be concluded that the annealing step did not alter the sample composition; in particular, the O contamination was the same before and after annealing, which is in agreement with the EPMA results. Nevertheless, the improvement of the superconducting properties could be clearly related to the transformation of niobium oxide into niobium oxynitride [39], as deduced from the XPS results. Additionally, as previously discussed, the grain growth induced by annealing could also contribute to the enhanced Tc. The understanding of each contribution requires further investigation.

With respect to the comparison of the plasma nature and duration, the H_2 plasma for 24 s is presumably the best compromise because it yields the optimal result before and after annealing. The oxynitride formation and resulting excellent Tc result may have originated from the formation of Nb in the metallic state during the hydrogen pulse (followed by the TBTDEN pulse), which is easily oxidized to form oxynitride. This latter point is supported by thermodynamic considerations using Factsage 7.2 thermodynamic software; the FactPS database demonstrates the strongest affinity for oxygen of niobium compared to that for niobium nitride:

$\Delta G_{reaction}$ (Nb->Nb_2O_5) = -944 kJ/at (@ 500 K)

$\Delta G_{reaction}$ (NbN->Nb_2O_5) = -711 kJ/at (@ 500 K).

Conclusions

In this study, we presented an ALD approach which consists of combining TBTDEN as the niobium precursor with a supercycle of plasma H_2 followed by a pulse of NH_3. The objective of this step was to break the TBTDEN ligands due to the H_2 plasma and to facilitate the surface chemical reaction with NH_3. The ALD window of this process was obtained between 350 and 380 °C with a GPC of 0.015 nm/cycle. Under these conditions, the NbN film density was 7 g/cm^3. At lower temperatures, the decomposition of TBTDEN did not complete as presumed from the XPS contribution in C 1s associated with the binding of Nb-C. The NbN films were also grown at 350 °C by a PEALD process of TBTDEN and NH_3 plasma and the effect of plasma duration was performed to enable comparison.

The superconducting properties of the as-deposited carbon-free NbN films were not satisfactory; hence, an annealing treatment in argon at 1000 °C was conducted. All the annealed samples exhibited a superconducting behavior with a Tc above 10 K. The optimum Tc (13.8 K) was obtained for a sample grown with the supercycle approach.

The structural characterization and variation in the chemical state of the elements in the film indicated that the improved Tc was due to a partial transformation of the niobium oxide into niobium oxynitride in the NbN film, with no change in the impurity level. However, the reduction of the grain boundaries induced by the grain growth cannot be excluded. Finally, the ability of an RF cavity to sustain thermal annealing should be investigated. The technical aspects of this heat treatment require consideration. We expected the NbN layer to function as a diffusion barrier to prevent the diffusion of Ar in Nb, which degrades the performance of the cavities [40].

Acknowledgements

The authors wish to thank S. Coindeau, H. Roussel, and T. Encinas for detailed discussions of the XRD results and C. Antoine and T. Proslier for discussions on the superconducting radio frequency device criteria. This work was supported by the Investments for the Future Program and was conducted within the framework of the Centre of Excellence of Multifunctional Architectured Materials [CEMAM, grant number ANR-10-LABX-44-01]. This work was also partly supported by EuCARD-2 (312453) project (Enhanced European Coordination for Accelerator Research & Development).

References

[1] M. Benkahoul, E. Martinez, A. Karimi, R. Sanjinés, F. Levy, Structural and mechanical properties of sputtered cubic and hexagonal NbN_x thin films, Surf. Coat. Technol. 180-181 (2004) 178-183. https://doi.org/10.1016/j.surfcoat.2003.10.040.

[2] X.-J. Chen, V. V. Struzhkin, Z. Wu, M. Somayazulu, J. Qian, S. Kung, A. N. Christensen, Y. Zhao, R. E. Cohen, H.-K. Mao,R. J. Hemley, Hard superconducting nitrides, Proc. Natl Acad. Sci. USA 102(9) (2005) 3198-3201. https://doi.org/10.1073/pnas.0500174102.

[3] C. Delacour, J. Claudon, J.-P. Poizat, B. Pannetier, V. Bouchiat, J.-C. Villegier, M. Tarkhov, A. Korneev, B. Voronov, G. Gol'tsman, Superconducting single photon detectors made by local oxidation with an atomic force microscope, Appl. Phys. Lett. 90 (2007) 191116.https://doi.org/10.1063/1.2738195.

[4] D. Hazra, N. Tsavdaris, S. Jeabar, A. Rimm, F. Blanchet, F. Mercier, E. Blanquet, C. Chapelier M. Hofheinz, Superconducting properties of very high quality NbN thin films grown by high temperature chemical vapor deposition, Supercond. Sci. Technol. 29 (2016) 105011-16. https://doi.org/10.1088/0953-2048/29/10/105011, https://arxiv.org/abs/1603.09635.

[5] T. Suntola, Atomic layer epitaxy, Thin Solid Films 216 (1992) 84-89. https://doi.org/10.1016/0040-6090(92)90874-B.

[6] A. Gurevich, Enhancement of rf breakdown field of superconductors by multilayer coating, Appl. Phys. Lett. 88 (2006) 12511-13. https://doi.org/10.1063/1.2162264.

[7] C. Antoine, J. C. Villegier, G. Martinet, Study of nanometric superconducting multilayers for RF field screening applications, App. Phys. Lett. 102 (2013) 102603. https://doi.org/10.1063/1.4794938.

[8] L. Hiltunen, M. Leskela, M. Makela, L. Niinisto, E. Nykanen, P. Soininen, Nitrides of titanium, niobium, tantalum and molybdenum grown as thin films by the atomic layer epitaxy method, Thin Solid Films 166 (1988) 149-154. https://doi.org/10.1016/0040-6090(88)90375-6.

[9] K.-E. Elers, M. Ritala, M. Leskelä, E. Rauhala, $NbCl_5$ as a precursor in atomic layer epitaxy, Appl. Surf. Sci. 82/83 (1994) 468-474, https://doi.org/10.1016/0169-4332(94)90260-7.

[10] M. Ritala, T. Asikainen, M. Leskelä, J. Jokinen, R. Lappalainen, M. Utriainen, L. Niinist,E. Ristolainen, Effects of intermediate zinc pulses on properties of TiN and NbN films deposited by atomic layer epitaxy, Appl. Surf. Sci. 120 (1997) 199-212. https://doi.org/10.1016/S0169-4332(97)00387-5.

[11] T. Proslier, J. A. Klug, N. C. Becker, J. W. Elam, and M. J. Pellin, Atomic layer deposition of superconductors, ECS Trans. 41 (2011) 237-24. https://doi.org/10.1149/1.3633673.

[12] M. Ritala, P. Kalsi, D. Riihelä, K. Kukli, M. Leskelä, J. Jokinen, Controlled Growth of TaN, Ta_3N_5, and TaO_xN_y Thin Films by Atomic Layer Deposition, Chem. Mater. 11 (1999) 1712-1718. https://doi.org/10.1021/cm980760x.

[13] S. B. S. Heil, J. L. van Hemmen, C. J. Hodson, N. Singh, J. H. Klootwijk, F. Roozeboom, M. C. M. van de Sanden, W. M. M. Kessels, Deposition of TiN and HfO_2 in a commercial 200 mm remote plasma atomic layer deposition reactor, J. Vac. Sci. Technol. A25 (2007) 1357-1366. https://doi.org/10.1116/1.2753846.

[14] M. Ziegler, L. Fritzsch, J. Day, S. Linzen, S. Anders, J. Toussaint, H.-G. Meyer, Superconducting niobium nitride thin films deposited by metal organic plasma-enhanced atomic layer deposition, Supercond. Sci. Technol. 26 (2013) 025008-13. https://doi.org/10.1088/0953-2048/26/2/025008.

[15] M. Ziegler, S. Linzen, S. Goerke, U. Brückner, J. Plentz, J. Dellith, A. Himmerlich, M. Himmerlich, U. Hübner, S. Krischok, H.-G. Meyer, Effects of Plasma Parameter on Morphological and Electrical Properties of Superconducting Nb-N Deposited by MO-PEALD, IEEE Trans. Appl. Supercond. 27 7 (2017) 7501307. https://doi.org/10.1109/TASC.2017.2744326.

[16] E. Deguns, M Sowa, M Dalberth, R Bhatia, R Kanjolia, Plasma-Enabled ALD of niobium nitride using an organometallic Nb precursor, Proc. 218th Int. Conf. Electrochem. Soc. (2010) 177-182. https://doi: 10.1149/1.3485254.

[17] M. J. Sowa, Y. Yemane, J. Zhang, J. C. Palmstrom, L. Ju, N. C. Strandwitz, F. B. Prinz, J. Provine, Plasma-Enabled ALD of niobium nitride using an organometallic Nb precursor, J. Vac. Sci. Technol. A 35 (2017) 01B143. https://doi: 10.1149/1.3485254.

[18] S. Linzen, M. Ziegler, O.V. Astafiev, M. Schmelz, U. Hübner, M. Diegel, E. Il'ichev, H.G. Meyer, Structural and electrical properties of ultrathin niobium nitride films grown by atomic layer deposition, Supercond. Sci. Technol. 30 (2017) 3 35010. https://doi.org/10.1088/1361-6668/aa572a.

[19] M. Ukibe, G. Fujii, Superconducting characteristics of NbN films deposited by atomic layer deposition, IEEE Trans. Appl. Supercond. 27 (2017) 4 2201404 1-4. https://doi.org/10.1109/TASC.2017.2655719.

[20] N. Pessall, R.E.Gold, H.A.Johansen, A study of superconductivity in interstitial compounds, J. Phys. Chem. Solids, 29 (1968) 1 19-38. https://doi.org/10.1016/0022-3697(68)90251-5.

[21] A. Shoji, Fabrication of all-NbN Josephson tunnel junctions using single crystal NbN films for the base electrodes, IEEE Transactions on Magnetics 27 (1991) 2 3184-3187. DOI: 10.1109/20.133888

[22] T. Francavilla, S. Wolf, E. Skelton, Superconducting properties of reactively sputtered NbCN thin films, IEEE Transactions on Magnetics 17 (1981) 1 569-572. DOI: 10.1109/TMAG.1981.1061147

[23] R. Roy, P. F. Carcia, R. Messier, D. Rogowski,The effect of composition on the superconducting transition temperature in NbNxOy, Mater. Res. Bull. 10 (1975) 5 379-382. https://doi.org/10.1016/0025-5408(75)90008-2

[24] T. Motohashi, M. Ito, Y. Masubuchi, M. Wakeshima, S. Kikkawa, Crystal Structure and Superconducting Properties of Hexagonal Lithium–Niobium Oxynitride, Inorg. Chem. 51 (2012) 20, 11184-1118. https://doi.org/10.1021/ic301870n.

[25] Y.Ohashi,Y.Masubuchi, D.Venkateshwarlu, V.Ganesan, J.V.Yakhmi, T.Yoshida, S.Kikkawa, Local structure around the flux pinning centers in superconducting niobium silicon oxynitride (Nb0.87Si0.09□0.04)(N0.87O0.13), J. Solid state chem., 210 (2014) 1 238-241. https://doi.org/10.1016/j.jssc.2013.11.034.

[26] L. Tian, S. Ponton, M. Benz, A. Crisci, R. Reboud, G. Giusti, F. Volpi, L. Rapenne, C. Vallée, M. Pons, A. Mantoux, C. Jiménez, E. Blanquet, Aluminum nitride thin films deposited by hydrogen plasma enhanced and thermal atomic layer deposition, Surf. Coat. Technol. 347 (2018) 181-190. https://doi.org/10.1016/j.surfcoat.2018.04.031.

[27] J. Hinz, A J Bauer, L Frey, Analysis of NbN thin film deposition by plasma-enhanced ALD for gate electrode application, Semicond. Sci. Technol. 27 (2010) 7 075009. https://doi.org/10.1088/0268-1242/25/7/075009.

[28] Handbook of Inorganic Compounds, edited by D. L. Perry, CRC Press, Boca Raton, 2016.https://doi.org/10.1201/b10908.

[29] G.J. Kovács, I. Bertóti, G. Radnóczi, X-ray photoelectron spectroscopic study of magnetron sputtered carbon–nickel composite films, Thin Solid Films 516 (2008) 7942-7946. https://doi.org/10.1016/j.tsf.2008.06.005.

[30] A.N. Christensen, Preparation and structure of stoichiometric δ-niobium nitride, Acta Chem. Scand. A31 (1977) 77-78. https://doi.org/10.3891/acta.chem.scand.31a-0077.

[31] M. Hatano, T. Nishino, U. Kawabe, Effects of thermal annealing on superconducting Nb and NbN films, J. Vac. Sci. Technol. A 6 (1988) 4 2381-2385. https://doi.org/10.1116/1.575559.

[32] G.-I. Oya, Y. Onodera, Transition temperatures and crystal structures of single-crystal and polycrystalline NbNx films, J. Appl. Phys. 45 (1974) 1389-1397. https://doi.org/10.1063/1.1663418.

[33] Y. M. Shy, L. E. Totht, R. Somasundaram, Superconducting properties, electrical resistivities, and structure of NbN thin films, J. Appl. Phys. 44 (1973) 5539-5545. https://doi.org/10.1063/1.1662193.

[34] M. Guziewicz, W. Slysz, M. Borysiewicz, R. Kruszka, Z. Sidor, M. Juchniewicz, K. Golaszewska, J.Z. Domagala, W. Rzodkiewicz, J. Ratajczak, J. Bar, M. Wegrzecki, R. Sobolewski, Technology of ultrathin NbN and NbTiN films for superconducting photodetectors, Acta Phys. Polonica A 120 (2011) 76-79. https://doi.org/10.12693/APhysPolA.120.A-76.

[35] Z. Wang, A. Kawakami, Y. Uzawa, B. Komiyama, Superconducting properties and crystal structures of single-crystal niobium nitride thin films deposited at ambient substrate temperature, J. Appl. Phys. 79 10 (1996) 7837-7842. https://doi.org/10.1063/1.362392.

[36] L. Kang, P.H. Wu, J.R. Sh, W.X. Cai, S.Z. Yang, Z. M. Ji, Z. Wang, Fabrication and characterization of NbN, AlN and NbN/AlN/NbN on MgO substrates, Supercond. Sci. Technol. 16 (2003) 1417-1421. https://doi.org/10.1088/0953-2048/16/12/021.

[37] M. Kidszun, R. Huhne, B. Holzapfel, L. Schultz, Ion-beam-assisted deposition of textured NbN thin films, Supercond. Sci. Technol. 23 (2010) 025010. https://doi.org/10.1088/0953-2048/23/2/025010.

[38] J. Halbritter, A. Darlinski, Angle-resolved XPS studies of oxides at NbN, NbC, and Nb surfaces, Surf. Interface Anal. 10 5 (1987) 223–237. https://doi.org/10.1002/sia.740100502.

[39] G. Brauer, R. Esselborn, Oxidnitride als Katalysatoren zur Methanaktivierung, Z. anorg. allg. Chemie 308 1961 1-6 52–61. http://dx.doi.org/10.14279/depositonce-3014.

[40] A. Grassellino, A Romanenko, D Sergatskov, O Melnychuk, Y Trenikhina, A Crawford, A Rowe, M Wong, T Khabiboulline, F Barkov, Nitrogen and argon doping of niobium for superconducting radio frequency cavities: a pathway to highly efficient accelerating structures, Supercond. Sci. Technol. 26 (2013) 102001. https://iopscience.iop.org/article/10.1088/0953-2048/26/10/102001.

Figure captions

Fig 1 Growth per cycle (GPC) and density of the NbN films deposited on the Si substrates by PEALD as a function of the substrate temperature. Plasma power: 2800 W, H_2 flow rate: 80 mL/min. The other growth conditions are listed in Table 1 process 1.

Fig 2 C 1s peak of the as-grown NbN samples deposited at 330 and 350 °C by process 1 (with H_2 and NH_3 plasma.), and at 350 °C by process 2 (with NH_3 plasma). The XPS characterization was performed on the samples etched by Ar ions for 5 min to remove the oxide and contamination on the top surface.

Fig. 3 θ/2θ X-ray diffraction pattern of samples S1, S2, S3, and S4. Samples were tilted by 2° to decrease the silicon contribution.

Fig. 4 (a) Bright-field HRTEM image of the as-grown S2 sample. (b) Bright-field HRTEM image of the S2 sample annealed at 1000 °C for 30 min in Ar. (c) SAED pattern of the as grown sample sample (same sample than a)) compared to the theoretical pattern for the NbN cubic structure. (d) SAED pattern of the S2 annealed at 1000°C for 30 min in Ar sample (same sample than b)).

Fig. 5 Tc measurement of samples S1 to S4 after annealing in argon at 1000 °C for 30 min

Fig. 6 SEM morphology of the sample S2: (a) as-grown and (b) after annealing in argon at 1000 °C for 30 min

Fig. 7 θ/2θ X-ray diffraction pattern using a 2° tilt of samples S1–S4 after annealing in argon at 1000 °C for 30 min

Fig. 8 Lattice parameters calculated from the XRD patterns of samples S1–S4 before and after annealing in argon at 1000 °C for 30 min.

Fig. 9 Density of samples S1–S4 before and after annealing measured by XRR

Fig. 10 EPMA results of samples S1–S4 before and after annealing in argon at 1000 °C for 30 min: a) atomic ratio between Nb and N+O, b) oxygen atomic percentage.

Fig. 11 Core-level XPS spectrum of the Nb 3d and O 1s states of sample S2: a) as-grown and b) after annealing in argon at 1000 °C for 30 min. The Nb 3d spectra were fitted by three chemical states of Nb and the binding energies of Nb 3d5/2 are indicated.

Figure 1

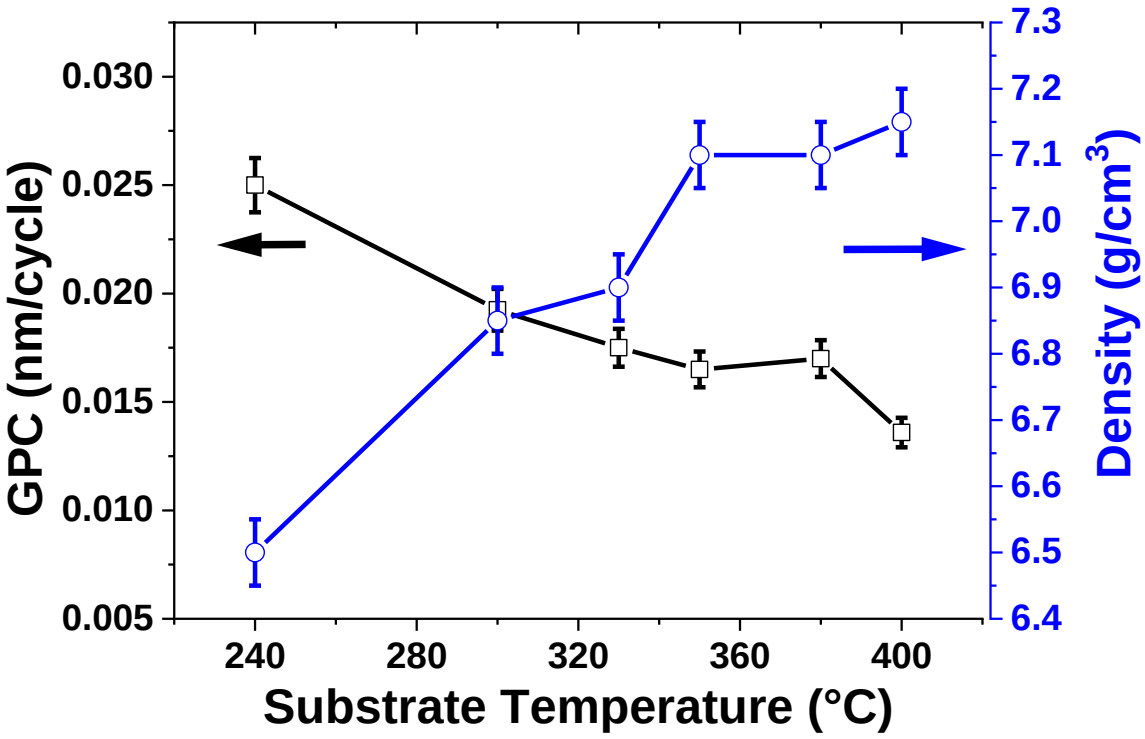
GPC (nm/cycle)
0.030
0.025
0.020
0.015
0.010
0.005
240
280
320
360
400
Substrate Temperature (°C)
7.3
7.2
7.1
7.0
6.9
6.8
6.7
6.6
6.5
6.4
Density (g/cm3)

Figure 2

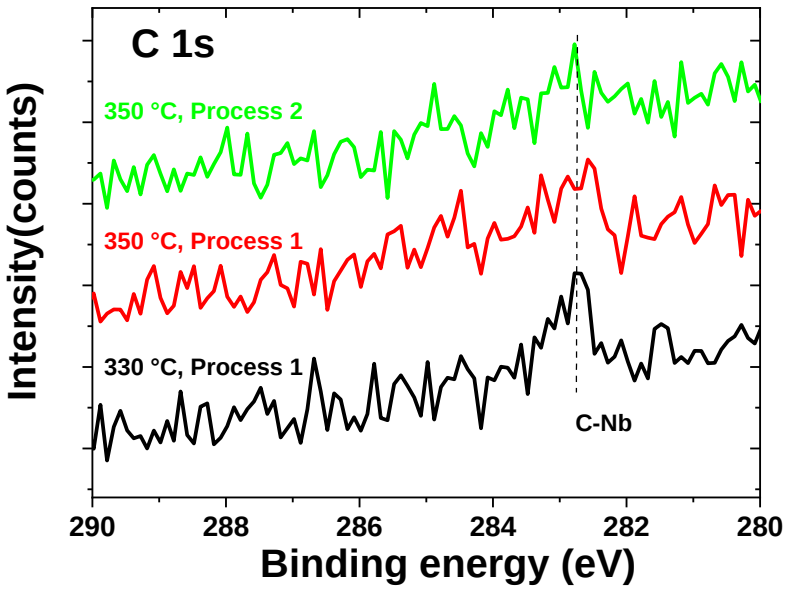
C 1s
350 °C, Process 2
350 °C, Process 1
330 °C, Process 1
C-Nb
Intensity(counts)
290
288
286
284
282
280
Binding energy (eV)

Figure 3

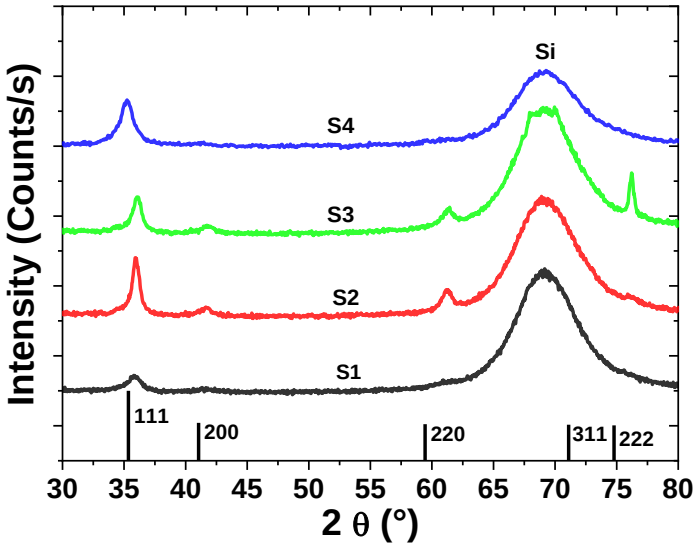
Intensity (Counts/s)
Si
S4
S3
S2
S1
111
200
220
311
222
30
35
40
45
50
55
60
65
70
75
80
2 θ (°)

Figure 4

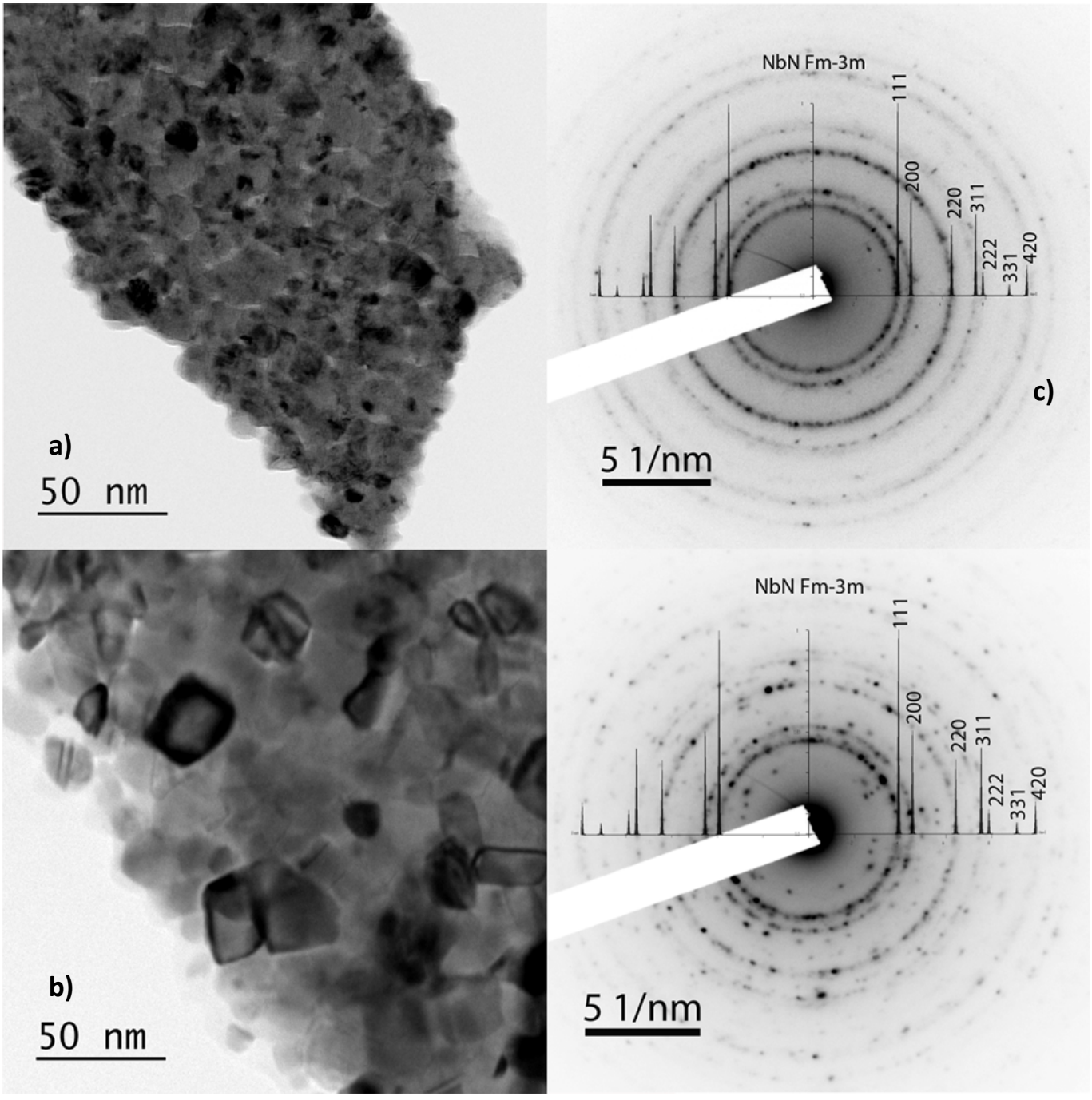
a)
50 nm
NbN Fm-3m
111
200
220
311
222
331
420
c)
5 1/nm
b)
50 nm
NbN Fm-3m
111
200
220
311
222
331
420
d)
5 1/nm

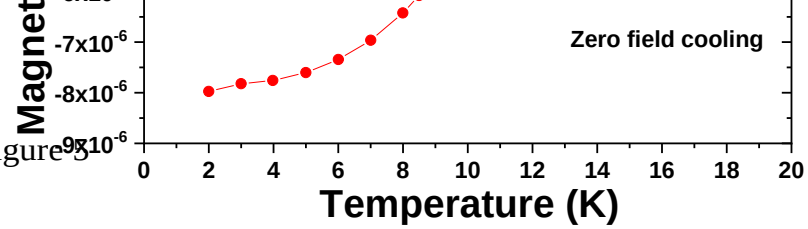
Magnet
-7x10-6
-8x10-6
-9x10-6
Zero field cooling
0
2
4
6
8
10
12
14
16
18
20
Temperature (K)

Figure 3

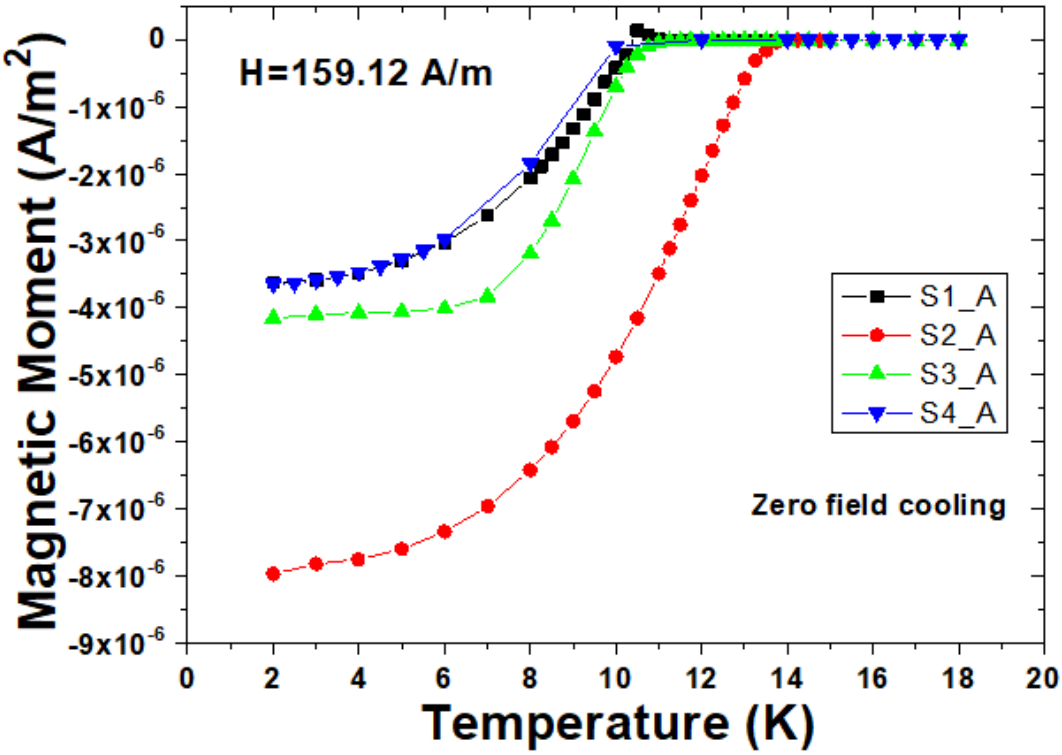
H=159.12 A/m
Magnetic Moment (A/m2)
0
-1x10-6
-2x10-6
-3x10-6
-4x10-6
-5x10-6
-6x10-6
-7x10-6
-8x10-6
-9x10-6
S1_A
S2_A
S3_A
S4_A
Zero field cooling
0
2
4
6
8
10
12
14
16
18
20
Temperature (K)

2-4

Figure 6

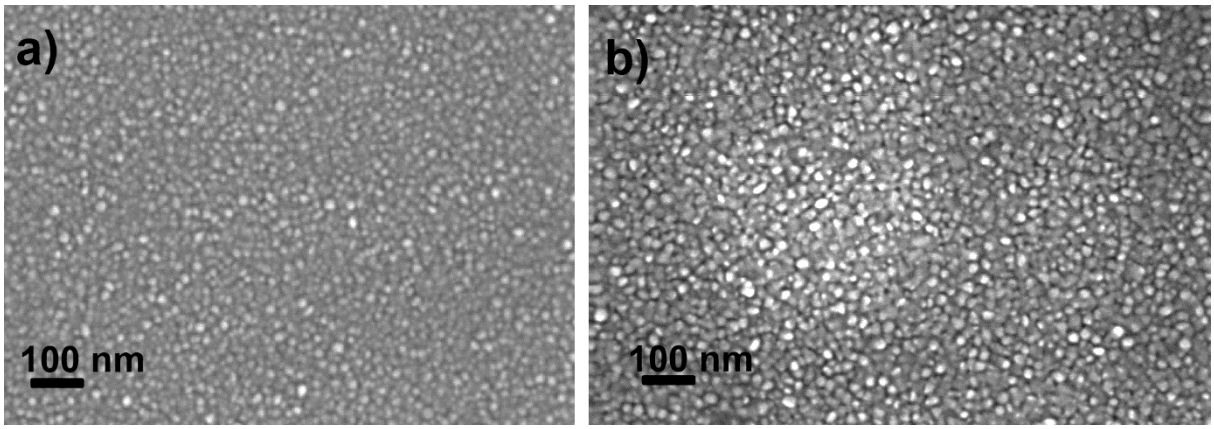

Figure 7

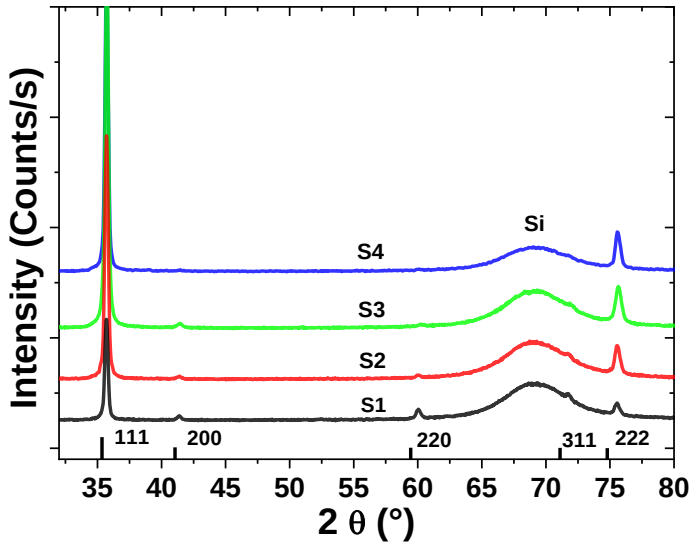
Intensity (Counts/s)
2 θ (°)
S4
S3
S2
S1
Si
111
200
220
311
222
35
40
45
50
55
60
65
70
75
80

Figure 8

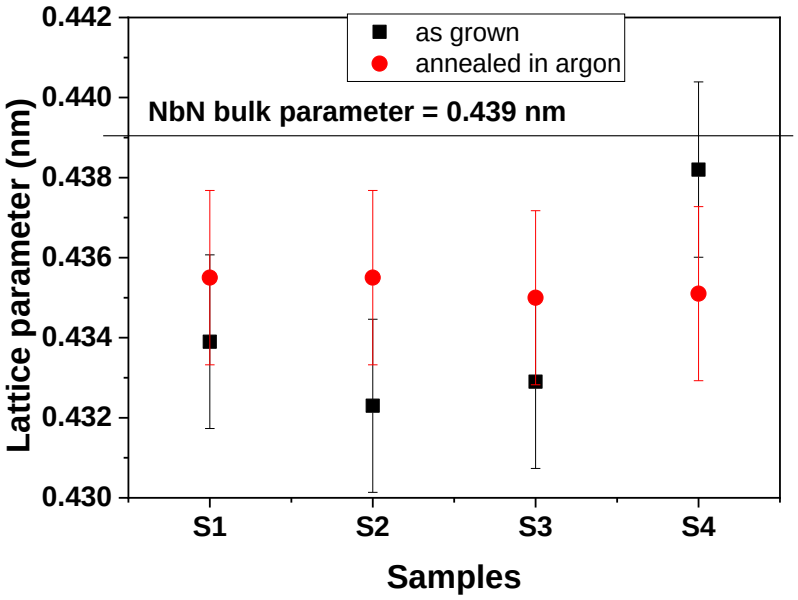
as grown
annealed in argon
NbN bulk parameter = 0.439 nm
Lattice parameter (nm)
0.442
0.440
0.438
0.436
0.434
0.432
0.430
S1
S2
S3
S4
Samples

Figure 9

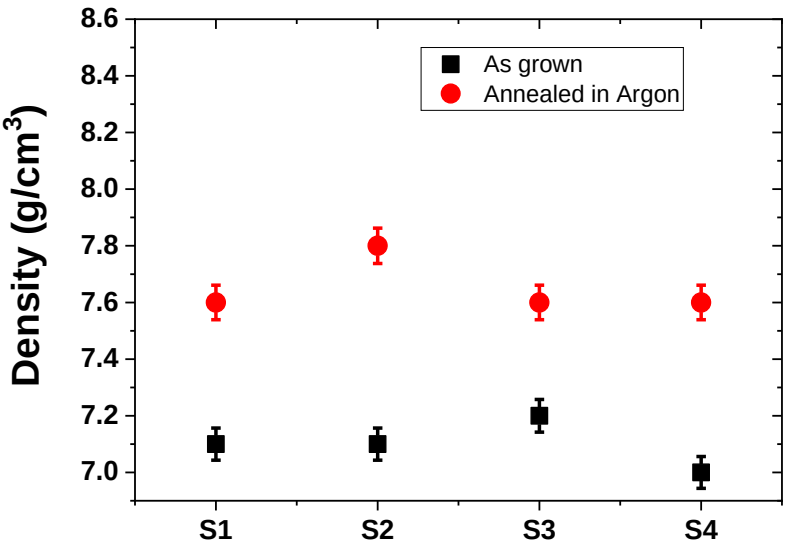
Density (g/cm^3)
8.6
8.4
8.2
8.0
7.8
7.6
7.4
7.2
7.0
S1
S2
S3
S4
As grown
Annealed in Argon

Figure 10

.

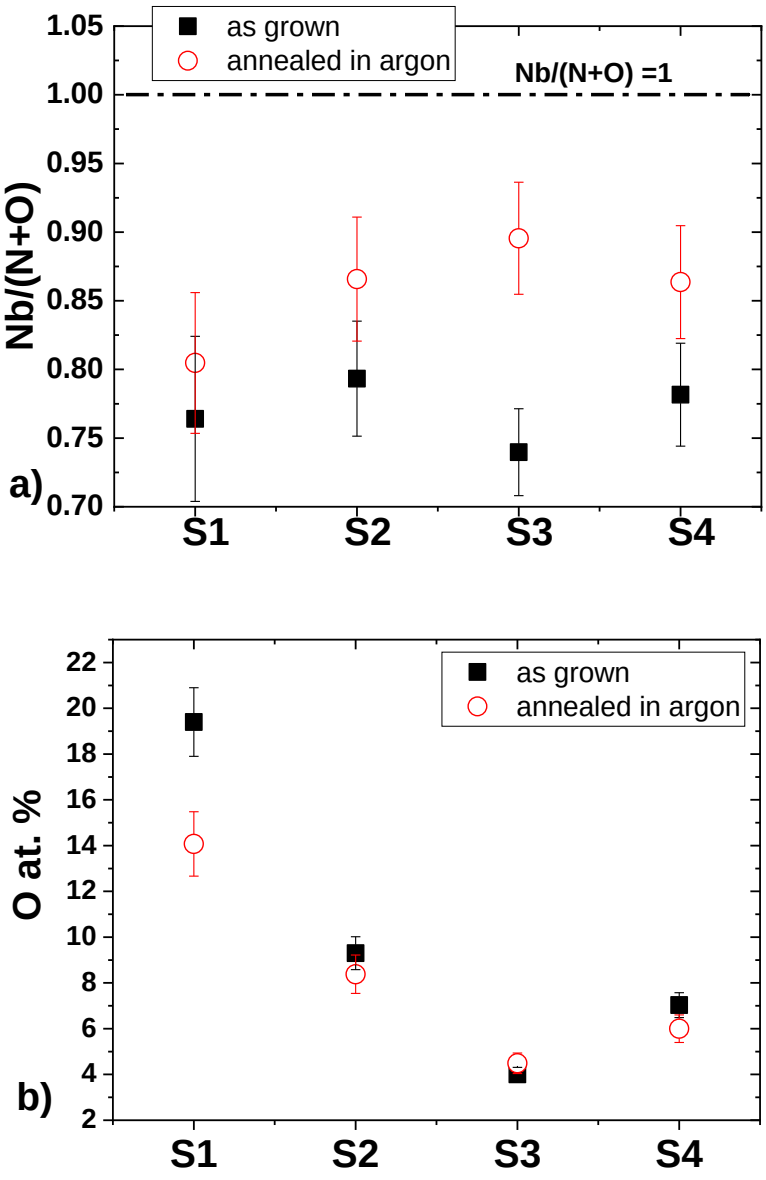
as grown
annealed in argon
Nb/(N+O) =1
Nb/(N+O)
1.05
1.00
0.95
0.90
0.85
0.80
0.75
0.70
a)
S1
S2
S3
S4
as grown
annealed in argon
O at. %
22
20
18
16
14
12
10
8
6
4
2
b)
S1
S2
S3
S4

Figure 11

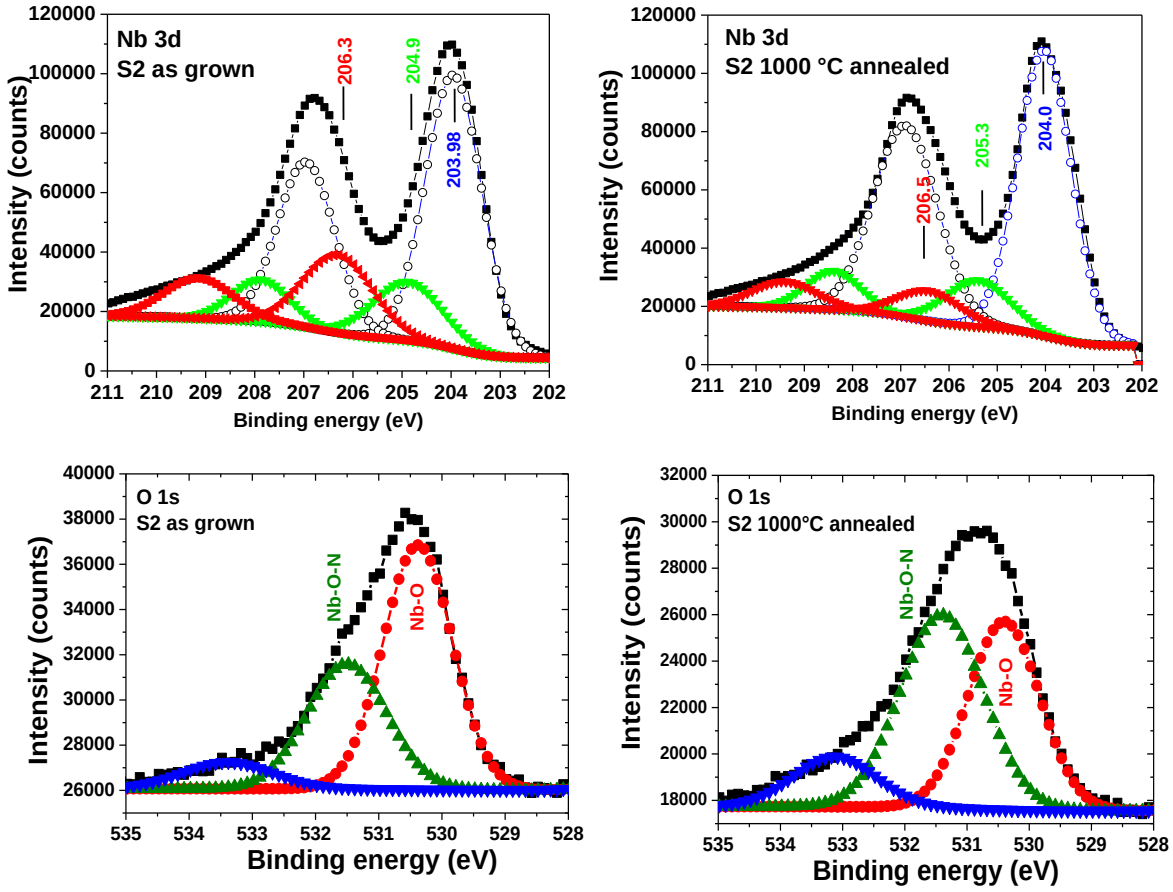
Nb 3d
S2 as grown
206.3
204.9
203.98
Intensity (counts)
Binding energy (eV)
Nb 3d
S2 1000 °C annealed
206.5
205.3
204.0
Intensity (counts)
Binding energy (eV)
O 1s
S2 as grown
Nb-O-N
Nb-O
Intensity (counts)
Binding energy (eV)
O 1s
S2 1000°C annealed
Nb-O-N
Nb-O
Intensity (counts)
Binding energy (eV)